Letters

Unveiling Starlink LEO Satellite OFDM-Like Signal Structure Enabling Precise Positioning

This letter unveils the unknown structure of Starlink low Earth orbit (LEO) satellites' orthogonal frequency division multiplexing (OFDM)-like reference signals (RSs). The spectrum of Starlink's downlink signals is presented, and the frame length is estimated. A blind receiver is proposed, which acquires via a sequential generalized likelihood ratio test multiple satellites, estimates their RSs and respective Doppler, and tracks their carrier and code phases. Experimental results are presented showing six tracked Starlink LEO satellites, three of which transmitted pure tones, whereas the other transmitted OFDM-like signals. The achieved horizontal positioning error with the six satellites was 6.5 m.

I. INTRODUCTION

Navigation with low Earth orbit (LEO) space vehicles (SVs) is receiving significant attention [1], [2], [3]. Research has shown that one could exploit LEO SVs' broadband communication signals opportunistically for navigation purposes [4].

The first positioning results with Starlink LEO SV signals were presented in [5] and [6]. These papers exploited a train of pure tones in the downlink of Starlink signals to obtain carrier phase and Doppler measurements. Starlink downlink signals occupy 250-MHz bandwidth of the *Ku*-band to provide high-rate broadband connectivity [7]. However, to the authors' knowledge, in the current literature, nothing beyond the pure tones transmitted in the downlink of Starlink SVs have been detected, tracked, and exploited for navigation purposes.

This letter unveils, for the first time, Starlink's orthogonal frequency division multiplexing (OFDM) reference signal (RS) structure, from which the frame length is estimated. Next, a blind receiver is proposed, which acquires multiple SVs, estimates their RSs and Doppler, and tracks their carrier and code phases. Upon processing the data collected in [6] from six Starlink LEO SVs via the proposed receiver, it turns out that while three of the SVs were transmitting pure tones, three were also transmitting OFDM-like signals. When the OFDM-like signals were fused into the

Manuscript received 22 October 2022; accepted 23 March 2023. Date of publication 10 April 2023; date of current version 12 April 2024.

DOI. No. 10.1109/TAES.2023.3265951

Refereeing of this contribution was handled by M. Baum.

This work was supported in part by the Office of Naval Research under Grant N00014-19-1-2511 and Grant N00014-22-1-2242, in part by the Air Force Office of Scientific Research (AFOSR) under Grant FA9550-22-1-0476, and in part by the U.S. Department of Transportation under Grant 69A3552047138 for the CARMEN University Transportation Center.

Authors' address: Mohammad Neinavaie and Zaher M. Kassas are with the Department of Electrical and Computer Engineering, The Ohio State University, Columbus, OH 43210 USA, E-mail: (zkassas@ieee.org). *(Corresponding author: Zaher M. Kassas.)*

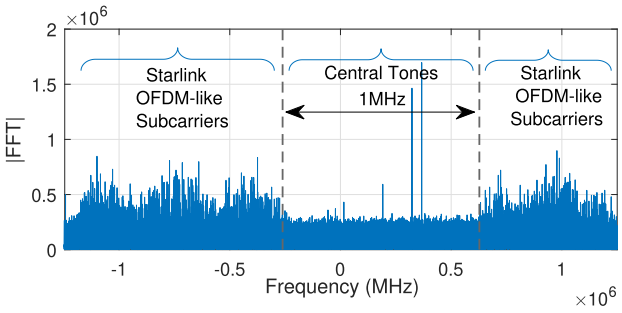

Fig. 1. Spectrum of Starlink downlink signals after Doppler rate wipe-off: OFDM-like subcarriers appeared along with central tones.

positioning framework, the horizontal positioning error is reduced from 10 m to 6.5 m.

II. RECEIVED SIGNAL MODEL

A. OFDM-Like Signal Frame Length

Starlink uses a 250-MHz signal bandwidth in the *Ku*-band for the satellite-to-user downlink [7]. Starlink SVs broadcast nine pure tones, which are approximately 43.9 kHz apart. In this letter, these tones are referred to as *central tones*, since they are located at the center of the 250-MHz bandwidth. At a first glance, a white signal containing the central tones is visible in the spectrum [5]. It should be pointed out that due to the high dynamics of Starlink SVs, the downlink signals suffer from Doppler rates, which can be on the order of thousands of Hz/s. The Doppler rate distorts the frequency components and imposes a whitening effect on the transmitted signals. Fig. 1 demonstrates the spectrum of Starlink downlink signals after the Doppler rate wipe-off. The details of the Doppler rate wipe-off process are provided in the following section. It can be seen that along with the central tones, OFDM-like subcarriers are also visible in the spectrum of Starlink downlink signals. OFDM signals contain frames in which some periodic RSs reside and are sent for synchronization purposes. The frame length, i.e., the period of the synchronization signals, can be obtained according to the autocorrelation function of a time segment of the received signal. The autocorrelation of a large enough time segment of the received signal will result in an impulse train, and the distances between two consecutive impulses are equal to the OFDM frame length. Fig. 2(a) demonstrates the autocorrelation of a 100-ms time segment of the Starlink downlink signal after Doppler rate wipe-off. It can be seen that the distance between the impulses of the resulting train is about 1.33 ms. Also, as a comparison, Fig. 2(b) shows the same processing on a 40-ms time segment of a 5G new radio (NR) signal, resulting in a frame length estimate of 10 ms, which matches the standard frame length of 5G NR downlink signals.

B. Baseband Signal Model

Based on the signal analysis in the previous section, the downlink signals from multiple Starlink SVs are modeled as unknown RSs of OFDM-like signals in the presence of noise [8]. Therefore, the received baseband signal samples

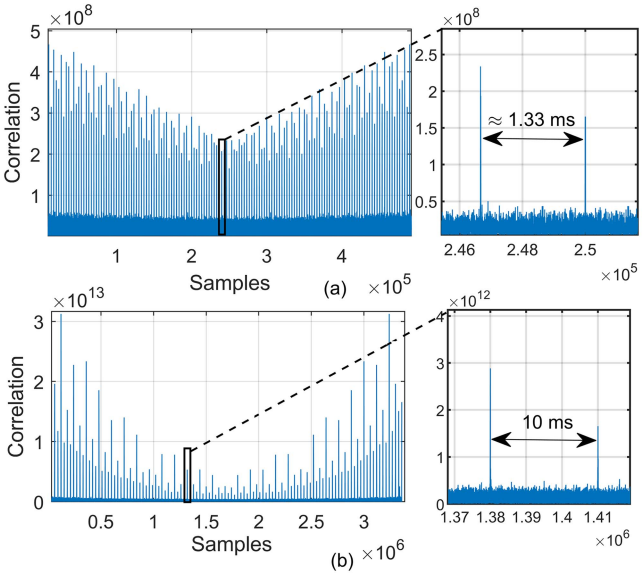

Fig. 2. Autocorrelation of the recorded signal after Doppler wipe-off. (a) Autocorrelation of 100 ms of Starlink downlink signal shows a frame length of about 1.33 ms. (b) Autocorrelation of 40 ms of 5G NR downlink signal, which shows the frame length of 10 ms (5G NR standard frame length).

can be written as

$$r[n] = \sum_{i=1}^{N} \alpha_i(\tau_n) c_i[\tau_n - t_{s_i}[n]] \exp\left(j\theta_i[\tau_n]\right) + w[n] \quad (1)$$

where $r[n]$ is the received signal at the nth time instant; N is the total number of Starlink SVs; $\alpha_i(\tau_n)$ is the complex channel gain between the receiver and ith Starlink SV; τ_n is the sample time expressed in receiver time; $c_i[n]$ represents samples of the complex periodic RS with a period of L samples; $t_{s_i}[n]$ is the instantaneous code-delay of the ith SV at the nth time instant; $\theta_i[\tau_n] = 2\pi f_{D_i}[n] T_s n$ is the carrier phase in radians, where $f_{D_i}[n]$ is the instantaneous Doppler frequency at the nth time instant and T_s is the sampling time; and $w[n]$ captures the effect of noise and transmitted data and is modeled as a complex zero-mean independent and identically-distributed Gaussian sequence with variance σ_w^2.

It is observed that during the processing interval, the instantaneous Doppler frequency $f_{D_i}[n]$ and the instantaneous code-delay $t_{s_i}[n]$ are almost linear functions of time; i.e., $f_{D_i}[n] = f_{D_i} + \beta_i n$ and $t_{s_i}[n] = t_{s_i} + \gamma_i n$; where f_{D_i} is referred to as Doppler, t_{s_i} is referred to as code-delay, β_i is the Doppler rate, and γ_i is referred to as the Doppler stretch corresponding to the ith Starlink SV. The coherent processing interval (CPI) is defined as the time interval in which the channel gain $\alpha_i(\tau_n)$, Doppler f_{D_i}, code-delay t_{s_i}, Doppler rate β_i, and Doppler stretch γ_i are all constant. The received signal at the nth time instant when the Doppler rate is wiped off is denoted by $r'[n] \triangleq \exp(-j2\pi\beta_i n^2) r[n]$. Assuming a constant Doppler rate, one can define $c_i'(\tau_n) \triangleq c_i[(1-\gamma_i)\tau_n - t_{s_i}]$. Due to the periodicity of the RS, $c'(\tau_n)$ is also periodic with period $L' \triangleq \frac{L}{1-\gamma_i}$. Moreover, one can define $s_i[n] \triangleq \alpha_i c'[\tau_n] \exp(j2\pi f_{D_i} T_s n)$

to obtain $r'[n] = \sum_{i=1}^{N} s_i[n] + w[n]$. Due to the periodicity of $c'(\tau_n)$, $s_i[n]$ has the following property:

$$s_i[n + mL'] = s_i[n] \exp\left(j\omega_i mL'\right), \quad 0 \le n \le L' - 1 \quad (2)$$

where $\omega_i = 2\pi f_{D_i} T_s$ is the normalized Doppler and $-\pi \le \omega_i \le \pi$. A vector of L' observation samples corresponding to the mth period of the signal is formed as $\mathbf{z}_m \triangleq [r'[mL'], r'[mL'+1], \ldots, r'[(m+1)L'-1]]^{\mathsf{T}}$. The CPI vector is constructed by concatenating K vectors of $\mathbf{z}_m$ to form the $KL' \times 1$ vector

$$\mathbf{y} = \sum_{i=1}^{N} \mathbf{H}_i \mathbf{s}_i + \mathbf{w} \quad (3)$$

where $\mathbf{s}_i = [s_i[1], s_i[2], \ldots, s_i[L']]^{\mathsf{T}}$; $\mathbf{H}_i \triangleq [\mathbf{I}_{L'}, \exp(j\omega_i L')\mathbf{I}_{L'}, \ldots, \exp(j\omega_i(M-1)L')\mathbf{I}_{L'}]^{\mathsf{T}}$ is a $KL' \times L'$ Doppler matrix with $\mathbf{I}_{L'}$ being an $L' \times L'$ identity matrix; and $\mathbf{w}$ is the noise vector.

III. RECEIVER STRUCTURE

This section presents the structure of the proposed receiver, consisting of two stages: 1) acquisition and 2) tracking.

A. Acquisition: Sequential Matched Subspace Detection

In this letter, the acquisition stage is formulated as a *sequential matched subspace detection* problem [9], [10]. The reader is referred to the work in [8] and [11] for further interpretations of matched subspace detectors. In the first step of the proposed sequential algorithm, the presence of a single Starlink SV is tested, and if the null hypothesis is accepted, then $\hat{N} = 0$, which means that no Starlink SV is detected to be present in the environment under the test. If the test rejects the null hypothesis, the algorithm asserts the presence of at least one source and performs the test to detect the presence of other SVs in the presence of the previously detected SVs, sequentially. The Doppler and RS of each SV are estimated at each step as follows.

In order to test the presence of $\mathbf{s}_i$ at the ith stage of the acquisition algorithm, the observation vector (3) can be written as $\mathbf{y} = \mathbf{H}_i\mathbf{s}_i + \mathbf{B}_{i-1}\boldsymbol{\theta}_{i-1} + \mathbf{w}$, where $\mathbf{B}_{i-1} \triangleq [\mathbf{H}_1, \mathbf{H}_2, \ldots, \mathbf{H}_{i-1}]$ and $\boldsymbol{\theta}_{i-1} \triangleq [\mathbf{s}_1^{\mathsf{T}}, \mathbf{s}_2^{\mathsf{T}}, \ldots, \mathbf{s}_{i-1}^{\mathsf{T}}]^{\mathsf{T}}$. The generalized likelihood ratio test for detecting $\mathbf{s}_i$ at each stage can be written as [8]

$$\mathcal{L}(\mathbf{y}) = \frac{\|\mathbf{H}_i^{\mathsf{H}}\mathbf{P}^{\perp}_{\mathbf{B}_{i-1}}\mathbf{y}\|^2}{\|\mathbf{P}^{\perp}_{\mathbf{B}_{i-1}}\mathbf{y}\|^2} \underset{\mathcal{H}_0^i}{\overset{\mathcal{H}_1^i}{\gtrless}} \eta_i \quad (4)$$

where $\mathcal{H}_1^i$ is the hypothesis that $\mathbf{s}_i$ is present at the ith stage of the acquisition, $\mathcal{H}_0^i$ is the hypothesis that $\mathbf{s}_i$ is absent, $\mathbf{y}^{\mathsf{H}}$ is the Hermitian transpose of $\mathbf{y}$, $\mathbf{P}_{\mathbf{X}} \triangleq \mathbf{X}(\mathbf{X}^{\mathsf{H}}\mathbf{X})^{-1}\mathbf{X}^{\mathsf{H}}$ denotes projection matrix to the column space of $\mathbf{X}$, and $\mathbf{P}^{\perp}_{\mathbf{X}} \triangleq \mathbf{I} - \mathbf{P}_{\mathbf{X}}$. The threshold η_i is a predetermined threshold at the ith stage. The maximum likelihood (ML) estimate of ω_i is obtained by maximizing the likelihood function under $\mathcal{H}_1^i$, which yields

$$\hat{\omega}_i = \arg\max_{\omega_i} \|\mathbf{H}_i^{\mathsf{H}}\mathbf{P}^{\perp}_{\mathbf{B}_{i-1}}\mathbf{y}\|^2 \quad (5)$$

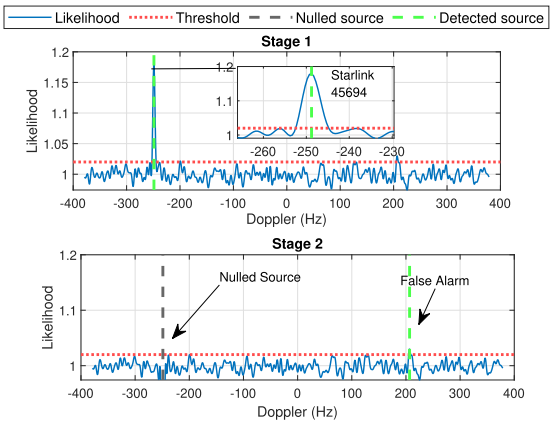

Fig. 3. Acquisition—Stage 1: Source at −249.288 Hz is detected. Stage 2: The first source is nulled and a source at 207.212 is detected.

and is used to construct $\mathbf{P}_{\mathbf{B}_{i-1}}$ and $\mathbf{H}_i$ used in the next stage (with $\mathbf{P}_{\mathbf{B}_0} \equiv \mathbf{I}$). The ML estimate of the ith Starlink RS $\mathbf{s}_i$, is given by $\hat{\mathbf{s}}_i = \frac{1}{\lambda_i}\mathbf{H}_i^{\mathsf{H}}\mathbf{P}^{\perp}_{\mathbf{B}_{i-1}}\mathbf{y}$, where $\lambda_i\mathbf{I} = \mathbf{H}_i^{\mathsf{H}}\mathbf{P}^{\perp}_{\mathbf{B}_{i-1}}\mathbf{H}_i$. If the null hypothesis at the ith stage of the sequential algorithm is accepted, the algorithm is terminated and the estimated number of Starlink SVs will be $\hat{N} = i - 1$.

B. Tracking

After obtaining coarse estimates of the Doppler frequencies and estimates of the RSs in the acquisition stage, the receiver refines and maintains these estimates via tracking loops. Specifically, phase-locked loops are employed to track the carrier phases of the detected RSs and carrier-aided delay-locked loops [12] are used to track the RSs' code phases as in [8]. Each detected source has its own dedicated tracking loop.

IV. EXPERIMENTAL RESULTS

This section presents experimental results showing the first precise positioning results that exploit Starlinks' OFDM-like signals. A stationary National Instrument universal software radio peripheral 2945R was equipped with a consumer-grade Ku antenna and a low-noise block downconverter to receive Starlink signals in the *Ku*-band. The sampling rate was set to 2.5 MHz and the carrier frequency was set to 11.325 GHz to record Ku signals over a period of 800 s. Six Starlink SVs were broadcasting nine pure tones during this period, and the algorithm detected OFDM-like signals in the downlink of three of these SVs. To avoid redundancy, the acquisition and tracking results of only one of the OFDM transmitting SVs are presented next.

A. Acquisition

The detection threshold was set $\eta_i = 1.02$ and K was set to 220. Doppler estimation was performed by searching for the maximizer of the likelihood function (5) with a step size of 1 Hz. The acquisition stages in the proposed receiver are illustrated in Fig. 3, where, in the first stage, one source is detected at frequency −249.288 Hz; in the second stage, another source is detected at 207.212 Hz; and finally, in the third stage, the Doppler subspace of the first two sources are

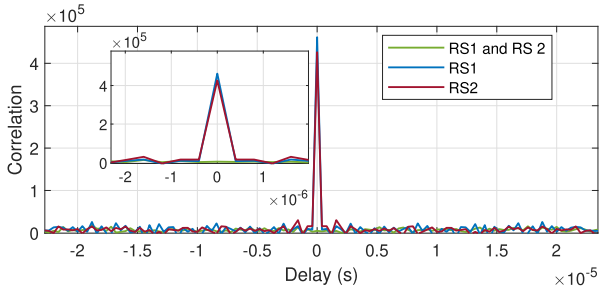

Fig. 4. Autocorrelation function of estimated RS of Starlink 45694 (RS 1), Starlink 45693 (RS 2), and their crosscorrelation function.

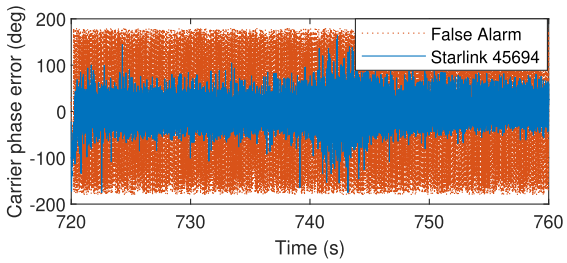

Fig. 5. Carrier phase error for the source at −249.288 Hz (Starlink 45694) and the source at 207.212 Hz (false alarm).

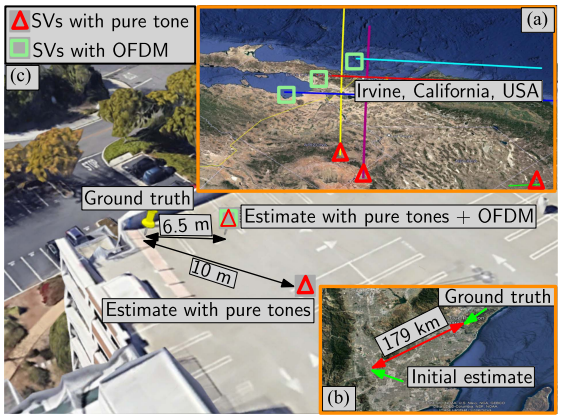

Fig. 6. (a) Starlink SVs trajectories. (b) Initial estimate relative to true position. (c) Positioning results with six Starlink SVs.

nulled and the resulting likelihood is less than the threshold, leading to $\hat{N} = 2$. It should be pointed out that the detected sources can be either an SV or a false alarm (multipath or other unwanted sources). It will be demonstrated in the next section that if at the acquisition stage, a false alarm occurs (i.e., a source is mistakenly detected), the carrier phase error will not converge in the tracking loops. In this case, the proposed receiver should neglect such a source. Fig. 4 demonstrates the correlation properties of the estimated RSs. The shape of the autocorrelation function reveals that all the available bandwidth ($\frac{1}{0.4\times10^{-6}} = 2.5$ MHz, in this experiment) is exploited.

B. Tracking

Fig. 5 demonstrates the carrier phase error for the two detected sources. It can be seen that the carrier phase error for the source located at 207.212 Hz is not converging. Hence, the proposed receiver rejects this source as a false alarm and excludes it. Six Starlink SVs were tracked using the proposed receiver. While all six SVs broadcasted pure tones, three of them also transmitted OFDM-like signals.

The receiver's position is estimated via weighted nonlinear least-squares (WNLS) from Doppler measurements extracted from the three SVs with pure tones and the three SVs with OFDM-like signals. The WNLS formulation is similar to that in [6]. The receiver's position estimate was initialized as the centroid of all SV positions, projected onto the surface of the Earth, yielding an initial position error of 179 km. Recall that the final horizontal position with the pure tones was shown in [6] to be 10 m. When the OFDM-based Doppler measurements are incorporated, the error was reduced to 6.5 m. The positioning results are summarized in Fig. 6.

MOHAMMAD NEINAVAIE, Member, IEEE
ZAHER M. KASSAS, Senior Member, IEEE
The Ohio State University, Columbus, OH USA

REFERENCES

[1] M. Hartnett, "Performance assessment of navigation using carrier Doppler measurements from multiple LEO constellations," Master's thesis, Dept. Elect. Comput. Eng., Wright-Patterson Air Force Base, Air Force Inst. Technol., Ohio, OH, USA, 2022.

[2] N. Jardak and Q. Jault, "The potential of LEO satellite-based opportunistic navigation for high dynamic applications," *Sensors*, vol. 22, no. 7, pp. 2541–2565, 2022.

[3] F. S. Prol et al., "Position, navigation, and timing (PNT) through low earth orbit (LEO) satellites: A survey on current status, challenges, and opportunities," *IEEE Access*, vol. 10, pp. 83971–84002, 2022.

[4] Z. Kassas, "Navigation from low earth orbit—Part 2: Models, implementation, and performance," in *Position, Navigation, and Timing Technologies in the 21st Century*, J. Morton, F. van Diggelen, J. Spilker, Jr., and B. Parkinson, Eds., vol. 2. Hoboken, NJ, USA: Wiley, 2021, ch. 43, pp. 1381–1412.

[5] J. Khalife, M. Neinavaie, and Z. M. Kassas, "The first carrier phase tracking and positioning results with Starlink LEO satellite signals," *IEEE Trans. Aerosp. Electron. Syst.*, vol. 56, no. 2, pp. 1487–1491, Apr. 2022.

[6] M. Neinavaie, J. Khalife, and Z. M. Kassas, "Acquisition, Doppler tracking, and positioning with Starlink LEO satellites: First results," *IEEE Trans. Aerosp. Electron. Syst.*, vol. 58, no. 3, pp. 2606–2610, Jun. 2022.

[7] I. D. Portillo, B. Cameron, and E. Crawley, "A technical comparison of three low earth orbit satellite constellation systems to provide global broadband," *Acta Astronautica*, vol. 159, pp. 123–135, 2019.

[8] M. Neinavaie, J. Khalife, and Z. M. Kassas, "Cognitive opportunistic navigation in private networks with 5G signals and beyond," *IEEE J. Sel. Topics Signal Process.*, vol. 16, no. 1, pp. 129–143, Jan. 2022.

[9] L. Scharf and B. Friedlander, "Matched subspace detectors," *IEEE Trans. Signal Process.*, vol. 42, no. 8, pp. 2146–2157, Aug. 1994.

[10] F. Gini and A. Farina, "Vector subspace detection in compound-Gaussian clutter. Part I: Survey and new results," *IEEE Trans. Aerosp. Electron. Syst.*, vol. 38, no. 4, pp. 1295–1311, Oct. 2002.

[11] H. Bolvardi, M. Derakhtian, and A. Sheikhi, "Dynamic clutter suppression and multitarget detection in a DVB-T-based passive radar," *IEEE Trans. Aerosp. Electron. Syst.*, vol. 53, no. 4, pp. 1812–1825, Aug. 2017.

[12] M. Braasch and A. Dempster, "Tutorial: GPS receiver architectures, front-end and baseband signal processing," *IEEE Aerosp. Electron. Syst. Mag.*, vol. 34, no. 2, pp. 20–37, Feb. 2019.